


## Order to Disorder Transition in a Coarsening Two-Dimensional Foam

Nicolas Taccoen,<sup>1</sup> Benjamin Dollet<sup>1,2</sup> and Charles N. Baroud<sup>1,3,\*</sup>

<sup>1</sup>LadHyX and Department of Mechanics, Ecole Polytechnique, CNRS, 91128 Palaiseau, France

<sup>2</sup>Université Grenoble Alpes, CNRS, LIPhy, 38000 Grenoble, France

<sup>3</sup>Physical microfluidics and Bioengineering, Institut Pasteur, 25-28 Rue du Dr. Roux, 75015, Paris, France

 (Received 1 August 2019; published 5 December 2019)

We quantify the spatiotemporal transformation of a monodisperse and well-ordered monolayer of bubbles, as they undergo Ostwald ripening, by tracking the size polydispersity of the bubbles and local ordering of the foam. After nuclei of disorder appear at random locations, the transition takes place through two successive phases: first, the disordered regions grow while the value of polydispersity increases slowly, then the polydispersity grows rapidly once the disordered zones begin to merge together. The transition is captured by a modified logistic model.

DOI: 10.1103/PhysRevLett.123.238006

Foams are self-organized assemblies of bubbles packed together in a continuous liquid phase. They present unusual mechanical [1–3], acoustical [4], and heat transfer properties [5]; in particular, they are excellent thermal insulators but dissipate mechanical energy very efficiently. The peculiar foam properties originate from their structure at the bubble scale. However, controlling this structure is challenging because it constantly evolves, owing to various dynamical processes. These processes can be (i) local, at the scale of individual bubbles, like gas transfer between neighboring bubbles, (ii) mesoscopic, like plastic rearrangements of bubbles that induce elastic stress redistribution in the foam nearby [6–8], and (iii) macroscopic at the scale of the complete foam, like gravitational drainage.

Understanding the aging of foams or emulsions is therefore of great relevance in many applications. This is particularly true for wet foams, in which the liquid fraction exceeds about 10%, which are widespread in food products, cosmetics, construction materials, fire fighting, or high performance materials [9]. This context has motivated much work on the time evolution of the bubble distribution in a foam. Particular attention has been paid to the transfer of gas between bubbles of different sizes, a mechanism known as Ostwald ripening [10–13]. This process leads small bubbles to dissolve into large ones and culminates with the disappearance of small bubbles while the average radius of the remaining bubbles increases. Statistical models for the late-time dynamics show that aging by Ostwald ripening is governed by self-similar dynamics, in which the bubble sizes converge to a stationary distribution, once rescaled by the average volume, which itself increases as a power law of time [14].

While monodisperse bubbles self-organize into a crystal structure that leads to specific physical and mechanical characteristics, this structure is lost when the bubbles become polydisperse. Although this transition corresponds

to a major change in the bubble structure and properties, the early-time aging of a monodisperse wet foam is not well understood. Indeed, most early-time studies have focused on dry foams, for which the evolution is dictated by pairwise gas transfer through thin films between neighboring bubbles. In contrast, gas transfer in wet foams takes place at several scales, owing to the large interstices of liquid between bubbles. Moreover, most of these existing studies have focused on testing [15] and extending [16] long predicted local features of the evolution, such as the so-called von Neumann, Lewis, or Aboav-Weaire laws (see Ref. [10] for a review).

Here we use microfluidics to generate a monolayer of monodisperse bubbles, using the confinement gradients approach [17] [see Fig. 1(a)]. In the device,  $3.3 \times 10^4$  bubbles of initial radius  $R_0 = 118 \mu\text{m}$  are produced in about 10 min and arrange into a monolayer on top of the

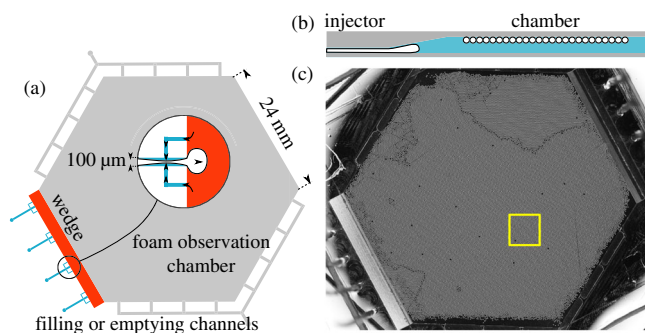


FIG. 1. (a) Sketch of the microfluidic device. A hexagonal chamber is connected to four air injectors. Height of red region increases from  $30 \mu\text{m}$  at the inlet to  $800 \mu\text{m}$  in the chamber. (b) Cross section of the chamber. The air injected through the slope breaks into monodisperse bubbles that pack atop the observation chamber. (c) Image of the device at the start of the experiment. The square indicates the area shown in the Figs. 2(a).

liquid layer [Figs. 1(b) and 1(c)]. The size and position of each bubble is then individually tracked for 20 h, which allows us to determine the time evolution of the complete monolayer; see materials and methods in Supplemental Material [18] for a detailed description of the experiment and protocol.

The foam initially exhibits a high crystalline order, the bubbles being hexagonally packed [Figs. 1(c), 2(a)(i)–2(a)(iv)]. Grain boundaries are present between regions of different crystal orientations and some vacancy defects are present. As time advances, some bubbles spontaneously begin to grow at the expense of their six immediate neighbors [Fig. 2(a)]. These disorder nuclei then begin to affect the following layer of neighbors [top two “rosettes” in Fig. 2(a)(ii)] and so on until the whole foam begins to look disordered and polydisperse. This process is summarized in Fig. 2(a) and in Movies M1 and M2 in Supplemental Material [18]. The ripening nuclei seem to appear randomly at different locations, independently of the position of the grain boundaries or of the vacancy defects.

This nucleation behavior is in marked contrast with dry 2D foams, where the number of neighbors determines the evolution of each bubble [23–26]. In the dry case, the number of neighbors constrains the curvature of the liquid films, which in turn dictates the pressures and thus the gas transfers between bubbles. This constraint is nonexistent in our case, since all the bubbles are spherical.

In parallel with the disordering of the monolayer, the distribution of bubble radii displays a continuous transition from a very peaked value at initial times to a broad distribution, a few hundred minutes later [Fig. 2(b)]. At late times, the normalized distribution reaches a stationary shape, which is the hallmark of the asymptotic self-similar

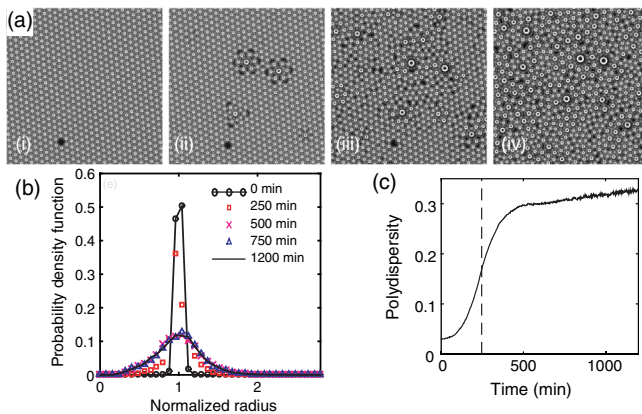


FIG. 2. (a) Close-up of the foam for  $t = 6, 126, 216,$  and  $291$  min. Note that the disorder does not nucleate near the vacancy defect. (b) Probability distributions of the bubble radii normalized by their mean value, for different times. Late-time size distributions collapse on a master curve. (c) Evolution of the total polydispersity  $\mathcal{P}$  of the foam. The vertical dashed line marks the position of the inflection point, at  $t = 246$  min.

dynamics, as predicted by the different models of Ostwald ripening [14]. Indeed, the exponents of the mean bubble radius  $\langle R \rangle$  and number of bubbles  $N$  are consistent with Lifshitz-Slyozov-Wagner theory [27,28], which predicts  $\langle R \rangle \sim t^{1/3}$  and  $N \sim t^{-1}$  (see Fig. S1 in Supplemental Material [18]) for a 3D dispersion of bubbles. This agreement on the long-term regime suggests that our monolayer system of spherical bubbles is a representative model system for a general 3D foam of nearly spherical bubbles.

The evolution of the size distribution can be quantified by tracking the polydispersity of the foam, defined as the ratio of the standard deviation to the mean of the bubble radii:  $\mathcal{P} = \sqrt{\langle (R - \langle R \rangle)^2 \rangle} / \langle R \rangle$ . The evolution of  $\mathcal{P}$  is represented in Fig. 2(c). It shows a transition from an initial monodisperse state ( $\mathcal{P} = 3\%$ ) to a state of steady polydispersity of around 30% at late times. The transition between the two states occurs through a sharp increase of  $\mathcal{P}$  between 100 and 400 min.

A breakdown of the crystalline arrangement accompanies the increase in polydispersity. This increase of spatial disorder can be quantified using a local order parameter, obtained by performing a Delaunay triangulation of the bubble positions, and distinguishing between regular, i.e., nearly equilateral, and irregular triangles (see Ref. [18] for details). By defining a threshold value for the order parameter, each bubble can be ascribed to the “ordered” versus “disordered” regions [Fig. 3(a)].

As described earlier [Fig. 2(a)], disordered regions nucleate as “rosettes,” then expand and merge together when their edges meet, as the disorder invades the foam. This leads to a final state in which the vast majority of the bubbles is classified as disordered. The ability of this classification to capture the dynamics of disorder growth is shown in Movie M3 in Supplemental Material [18], where the positions of the red dots (disorder) reproduce the locations of the most disordered zones, while the blue dots (ordered) correspond well to the hexagonal zones of the foam.

Based on this classification, it is possible to count the number of bubbles  $N_o$  in the ordered region and  $N_d$  in the disordered region, see Fig. 3(b) (subscripts  $o$  and  $d$  designating henceforth, respectively, ordered and disordered populations). Since  $N = N_o + N_d$  decreases, as tiny bubbles shrink and disappear, it is more representative to plot the number fraction of each class, defined as  $x \equiv x_d = N_d/N$  and  $x_o = N_o/N$ . The fraction of disordered bubbles is initially low and progressively increases [Fig. 3(b)]. At a crossover time of 246 min,  $x$  exceeds 50%, and quickly reaches nearly 100% of the population.

The division of the foam into ordered and disordered subpopulations allows us to calculate the two corresponding polydispersity coefficients  $\mathcal{P}_d$  and  $\mathcal{P}_o$ . Figure 3(c) shows that  $\mathcal{P}_d$  starts to grow earlier, and is always larger than  $\mathcal{P}_o$ . This intuitive result provides a quantitative link between the local changes in bubble size and the local

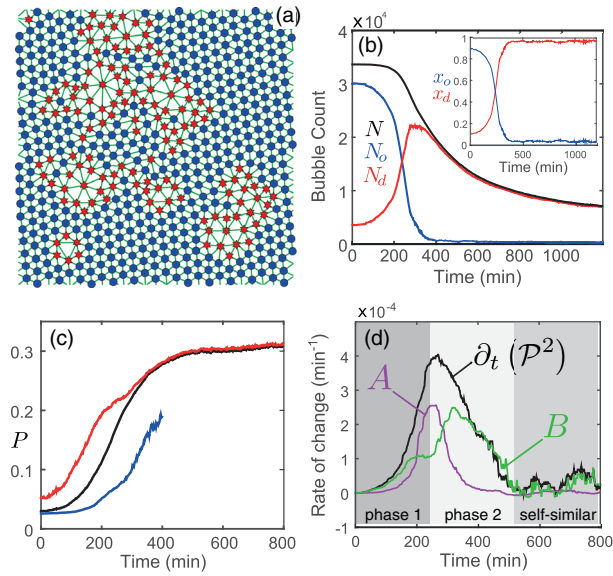


FIG. 3. (a) Delaunay triangulation of the bubbles of Fig. 2(a)(iii). Ordered bubbles are represented by blue disks, disordered ones by red stars. (b) Time evolution of the total number of bubbles  $N$  in the foam (black line), in the ordered population ( $N_o$ , blue line) and in the disordered population ( $N_d$ , red line). The inset shows the normalized fractions of bubbles in each class. (c) Evolution of the polydispersity of each population (red, disordered; blue, ordered; black, total). (d) Rate of change of  $\mathcal{P}^2$  (black curve) and its components: Curve A indicates the change in number of disordered bubbles while curve B indicates the increase in polydispersity for fixed values of  $x_d$  and  $x_o$  [see Eq. (2)].

disorder. The global evolution can then be obtained from a combination of the evolutions of the two subpopulations. If we assume that  $\langle R \rangle_o = \langle R \rangle_d$ , which is true at early times and remains approximately true afterwards (Fig. S2 [18]), we can compute  $\mathcal{P}$ :

$$\mathcal{P}^2 = x\mathcal{P}_d^2 + (1-x)\mathcal{P}_o^2. \quad (1)$$

The curve for  $\mathcal{P}$  shown in Fig. 3(c) indeed reproduces precisely the curve in Fig. 2 for the whole foam.

Equation (1) shows that an increase in the global polydispersity can be due either to an increase of the polydispersity within the disordered zone, for a fixed number fraction  $x$ , or to an increased size of the disordered zone at constant polydispersity. However, these two scenarios would have very different effects on the structure of the foam. To understand which effect dominates at any moment, we calculate the time derivative of Eq. (1):

$$\partial_t(\mathcal{P}^2) = \underbrace{\dot{x}(\mathcal{P}_d^2 - \mathcal{P}_o^2)}_A + \underbrace{x\dot{\mathcal{P}}_d^2 + (1-x)\dot{\mathcal{P}}_o^2}_B. \quad (2)$$

In this way we can distinguish the two aforementioned contributions: the first term (A) that describes the variation

of  $\mathcal{P}^2$ , due to the variation of the number of disordered bubbles  $\dot{x}$  at constant  $\mathcal{P}_d$  and  $\mathcal{P}_o$ , while the second term (B) characterizes the variations of the polydispersities of the two populations, for a given disorder fraction  $x$ .

As expected from the observed evolution of  $\mathcal{P}$ ,  $\partial_t(\mathcal{P}^2)$  displays a single peak [Fig. 3(d)]. However, it results from two different dynamical processes that occur successively. The first phase of growth is dominated by the A term of Eq. (2). It corresponds to the nucleation and growth of disorder, while the polydispersity in each of the zones increases slowly. This nucleation-growth phase takes place over a short and well-defined period. The second phase that follows is dominated by the B term; it lasts longer and displays a maximum that occurs after the expansion of the disordered regions has mostly decayed. This phase corresponds to the aging of the now globally disordered foam until the self-similar regime is reached.

Since the foam properties are intimately related to the spatial organization of the bubbles, the first stage profoundly alters the physical behavior of the foam. We therefore seek to understand the mechanisms governing the growth dynamics of the disordered zones, by modeling the evolution of  $x$ . To do so, we consider the growth of already formed nuclei of disorder, which invade the ordered regions at the boundaries between the two zones [Fig. 4(a)]. The rate of evolution of the fraction of disordered zones  $\dot{x}$  is expected to be proportional to the total perimeter of the boundaries between ordered and disordered zones. This perimeter is proportional to  $x(1-x)$  (Fig. S3 [18]),

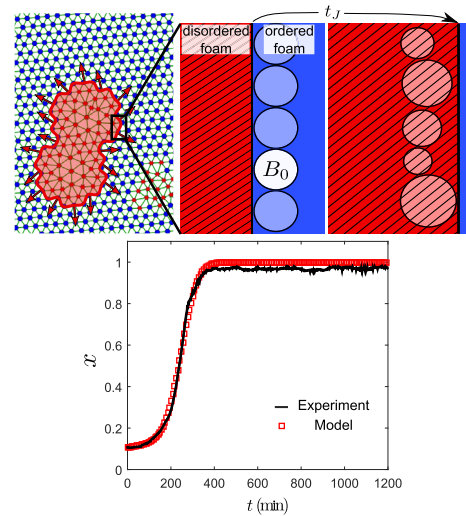


FIG. 4. Sketch of the model describing disorder invasion. (a) The ordered region (blue) is perfectly monodisperse, while the disordered region (red) has a known probability density function of bubble sizes. (b) Sketch of the dynamics that describes the increment of the border between the two regions by one row of bubbles. This is assumed to take place during a time  $t_f$ . (c) Time evolution of the disordered fraction  $x$ . The measured value (solid line) is very well reproduced by Eq. (5) with  $\tau_0 = 1.2 \times 10^2$  s as best fitting parameter.

indicating that the disordered regions are indeed randomly spatially distributed. We therefore expect the disordered regions to grow as  $\dot{x} = x(1-x)/\tau$ , where  $\tau$  is a characteristic invasion time.

The simplest model involves a constant value of  $\tau$ . This yields the well-known logistic equation, which has countless applications in the dynamics of populations, growth of tumors, and many other domains [29]. In the context of foams, a similar approach was used by Glazier *et al.* [15] for the coarsening of dry foams, except that these authors also accounted for the disappearance of small bubbles. The logistic equation has an analytical solution:  $x = x_0/[x_0 + (1-x_0)e^{-t/\tau}]$ , which can be fitted to our experimental data with  $\tau$  as a single fitting parameter. Although this captures the transition from an ordered to a disordered foam, it does not accurately capture the sharpness of the transition (Fig. S4 [18]).

We therefore question the assumption of a constant invasion time  $\tau$ , by considering the first row of ordered bubbles located at the edge of a disordered region. We assume that the radius of these bubbles begins to deviate from the initial value  $R_0$  as soon as the boundary of the disordered zone reaches them. They then switch to the disordered region when their radius changes sufficiently to locally break the crystalline arrangement. At this instant, they become disordered and the boundary jumps to the next row of bubbles, as depicted in Fig. 4. Similarly to the classical Lindemann criterion for the melting of crystals [30], we assume that this switch happens when the radius varies by a factor  $\alpha$ . Hence,  $\tau$  is taken as  $\tau = \alpha R_0 / |\dot{R}_0|$ .

The rate of variation of a bubble radius can be predicted by applying the Lemlich model [31,32] that uses a mean-field approximation to estimate the evolution of a particular bubble surrounded by a population of bubbles of random sizes. In our case, a bubble on the first ordered layer is exposed to the disordered environment on the other side of the boundary. According to the Lemlich formula, its rate of radius variation is

$$\dot{R}_0 = \kappa \left( \frac{1}{R_d^{21}} - \frac{1}{R_0} \right), \quad (3)$$

where  $\kappa$  is a parameter incorporating the physicochemical properties of the foam (see Ref. [18] for a detailed discussion). The radius  $R_d^{21}$  is the ratio of the second to the first raw moments of the size distribution of the disordered bubble population. Since here we consider only the distribution of disordered bubbles, its expression becomes

$$R_d^{21} = \frac{\langle R^2 \rangle_d}{\langle R \rangle_d} = \langle R \rangle_d (1 + \mathcal{P}_d^2), \quad (4)$$

by using the definition of the polydispersity.

We can now estimate the invasion time  $\tau$  from Eqs. (3) and (4). The sign of the radius variation is irrelevant, since

the disorder can arise from either shrinkage or swelling, so we take the absolute value of  $\dot{R}_0$ :  $1/\tau = (1/\alpha)|\dot{R}_0/R_0| = (\kappa/\alpha R_0)|1/[\langle R \rangle_d(1 - \mathcal{P}_d^2)] - (1/R_0)|$ . Finally, we recall that  $R_0 = \langle R \rangle_o \simeq \langle R \rangle_d$  (Fig. S2 of Ref. [18]), to obtain  $1/\tau = (\kappa/\alpha R_0)[\mathcal{P}_d^2/(1 + \mathcal{P}_d^2)] \simeq \mathcal{P}_d^2/\tau_0$  ( $\mathcal{P}_d \ll 1$ ), where  $\tau_0 = \alpha R_0^2/\kappa$ . This invasion rate can be inserted into the formula for  $\dot{x}$  and then integrated to yield:

$$x(t) = \left[ 1 - \left( 1 - \frac{1}{x_0} \right) \exp \left( -\frac{1}{\tau_0} \int_0^t \mathcal{P}_d(t')^2 dt' \right) \right]^{-1}. \quad (5)$$

The expression of Eq. (5) is fitted to the experimental measurement of  $x(t)$ , using the experimental values of  $\mathcal{P}_d$  as measured without further processing and taking  $\tau_0$  as a unique fitting parameter. As shown in Fig. 4, the agreement with the data is excellent, for a value of  $\tau_{0,\text{exp}} = 1.2 \times 10^2$  s. This agreement confirms that the destabilization of the foam is accelerated as the disordered regions become more polydisperse.

In order to compare the experimentally obtained value of  $\tau_{0,\text{exp}}$  with the theoretical estimate  $\tau_0 = \alpha R_0^2/\kappa$ , we return to the classical use of the Lindemann criterion. Indeed, the relative variation of radius  $\alpha$  necessary to induce local loss of order may be compared to the ratio  $\delta$  between the amplitude of thermal vibrations and the interatomic distance in a solid. This ratio has been measured for metals at the melting point:  $\delta = 0.07$  [33,34]. Therefore, taking  $\alpha = 0.07$  and using the values of  $\kappa$  in the Supplemental Material [18] yields  $\tau_0 = \alpha R_0^2/\kappa = 2.7 \times 10^2$  s. This value is in good agreement with the experimentally fitted parameter, even though the comparison between  $\alpha$  and  $\delta$  is only qualitative and despite the uncertainties on the values of the physical quantities.

The transition discussed above is both spatially inhomogeneous and takes place through two different dynamical processes. From a spatial point of view, the disorganization starts with the nucleation and growth of disordered regions that coexist with the ordered regions. The nuclei appear randomly everywhere in the monolayer and grow by incorporating the neighboring bubbles row by row. The global growth of the disordered regions follows an *accelerated* logistic model, in which the transition accelerates as the polydispersity increases. This growth then slows down when the disordered regions merge: this is evidenced by comparing the slowing-down of term  $A$  in Fig. 3(d) with the reduction in the perimeter of the disordered zones in Fig. S3 [18].

From a temporal point of view, the two successive periods correspond to different dynamics of the bubble monolayer. The first period, which corresponds to the switch from order to disorder, takes place for nearly constant number of bubbles and mean radius (Fig. S1 [18]). This contrasts with the second period, whose evolution is determined by the well-studied Ostwald

ripening dynamics: a decrease of the number of bubbles, as small bubbles disappear, and the corresponding increase in the mean radius of the remaining bubbles. Indeed, our measurements show very good agreement with the power laws predicted by the Lifshitz-Slyozov-Wagner theory. Interestingly, the duration of the first phase is expected to be independent of the total size of the foam, since it is given by the time required for the disordered regions to meet and merge. Since the disordered regions nucleate randomly and grow based on local equilibria, the total size of the foam is not expected to matter.

The dynamics discussed above bears a direct relation with industrial foams and emulsions, for which the scenario of nucleation and growth of disorder is expected to be preserved, the aging mechanisms for emulsions being also governed by the same physics. This implies that initially monodisperse systems should undergo periods of coexistence between ordered and disordered domains, each of which having distinct physical properties. The nuclei of disorder occur in the bulk of the foam, not only at its boundaries, and invade the whole system over a rather short and well-defined period. Knowing these mechanisms should have direct practical impact, for example, in choosing the timescale for solidifying the liquid phase to produce a solid foam. More interestingly, the coexistence state can in principle be used to create complex metafoams or metaemulsions, in which crystalline domains are randomly interspersed with amorphous domains. Controlling the interpenetration of the two domain types could allow materials with exotic mechanical, optical, or acoustic properties.

The authors acknowledge useful discussions with Eric Weeks and François Graner. The research leading to these results received funding from the European Research Council (ERC) Grant Agreement No. 278248 “Multicell.”

---

\*baroud@ladhyx.polytechnique.fr

- [1] A. D. Gopal and D. J. Durian, *Phys. Rev. Lett.* **91**, 188303 (2003).
- [2] S. Cohen-Addad, R. Höhler, and Y. Khidas, *Phys. Rev. Lett.* **93**, 028302 (2004).
- [3] B. Dollet and C. Raufaste, *C.R. Phys.* **15**, 731 (2014).
- [4] J. Pierre, B. Dollet, and V. Leroy, *Phys. Rev. Lett.* **112**, 148307 (2014).
- [5] Y. Arii and K. Nishizawa, *Bioscience, biotechnology, and biochemistry* **81**, 779 (2017).
- [6] J. Goyon, A. Colin, G. Ovarlez, A. Ajdari, and L. Bocquet, *Nature (London)* **454**, 84 (2008).
- [7] K. W. Desmond and E. R. Weeks, *Phys. Rev. Lett.* **115**, 098302 (2015).
- [8] B. Dollet, A. Scagliarini, and M. Sbragaglia, *J. Fluid Mech.* **766**, 556 (2015).
- [9] P. Stevenson, *Foam Engineering: Fundamentals and Applications* (Wiley, New York, 2012).
- [10] J. Stavans, *Rep. Prog. Phys.* **56**, 733 (1993).
- [11] D. Weaire and S. Hutzler, *The Physics of Foams* (Oxford University Press, New York, 1999).
- [12] A. Saint-Jalmes, *Soft Matter* **2**, 836 (2006).
- [13] K. Khakalo, K. Baumgarten, B. P. Tighe, and A. Puisto, *Phys. Rev. E* **98**, 012607 (2018).
- [14] J. Lambert, R. Mokso, I. Cantat, P. Cloetens, J. A. Glazier, F. Graner, and R. Delannay, *Phys. Rev. Lett.* **104**, 248304 (2010).
- [15] J. A. Glazier, S. P. Gross, and J. Stavans, *Phys. Rev. A* **36**, 306 (1987).
- [16] J. Duplat, B. Bossa, and E. Villiermaux, *J. Fluid Mech.* **673**, 147 (2011).
- [17] R. Dangla, S. C. Kayi, and C. N. Baroud, *Proc. Natl. Acad. Sci. U.S.A.* **110**, 853 (2013).
- [18] See Supplemental Material at <http://link.aps.org/supplemental/10.1103/PhysRevLett.123.238006> for more details on materials and methods, Delaunay triangulation and Lemlich model, as well as supplementary figures and movies, which includes Refs. [19–22].
- [19] D. J. Bray, S. G. Gilmour, F. J. Guild, and A. C. Taylor, *J. R. Stat. Soc.* **61**, 253 (2012).
- [20] N. Otsu, *IEEE Trans. Syst. Man Cybernet.* **9**, 62 (1979).
- [21] H. Princen and S. Mason, *J. Colloid Sci.* **20**, 353 (1965).
- [22] R. Sander, *Atmos. Chem. Phys.* **15**, 4399 (2015).
- [23] B. Levitan, *Phys. Rev. Lett.* **72**, 4057 (1994).
- [24] C. Sire, *Phys. Rev. Lett.* **74**, 3708 (1995).
- [25] Y. Jiang, J. C. M. Mombach, and J. A. Glazier, *Phys. Rev. E* **52**, R3333 (1995).
- [26] W. Tam, *Phys. Rev. E* **58**, 8032 (1998).
- [27] I. Lifshitz and V. Slyozov, *J. Phys. Chem. Solids* **19**, 35 (1961).
- [28] P. W. Voorhees, *J. Stat. Phys.* **38**, 231 (1985).
- [29] J. D. Murray, *Mathematical Biology: I. An Introduction*, 3rd ed. (Springer, New York, 2002).
- [30] F. A. Lindemann, *Phys. Z.* **11**, 609 (1910).
- [31] R. Lemlich, *Ind. Eng. Chem. Fundam.* **17**, 89 (1978).
- [32] N. Taccoen, F. Lequeux, D. Z. Gunes, and C. N. Baroud, *Phys. Rev. X* **6**, 011010 (2016).
- [33] S.-A. Cho, *J. Phys. F* **12**, 1069 (1982).
- [34] X. Zheng and J. Earnshaw, *Europhys. Lett.* **41**, 635 (1998).